EIGHTEENTH EUROPEAN ROTORCRAFT FORUM

B - 14

Paper No. 136

AN EXAMINATION OF THE EFFECTS OF BLADE-VORTEX INTERACTION ON FLOWS NEAR THE BLADE TIP

M.B. HORNER, R.A.McD. GALBRAITH
UNIVERSITY OF GLASGOW
GLASGOW, SCOTLAND

September 15-18, 1991

AVIGNON, FRANCE

ASSOCIATION AERONAUTIQUE ET ASTRONAUTIQUE DE FRANCE

AN EXAMINATION OF THE EFFECTS OF BLADE-VORTEX INTERACTION ON FLOWS NEAR THE BLADE TIP

M.B. Horner, R.A.McD. Galbraith
University of Glasgow
Glasgow, Scotland

1 Abstract

The experimental results of a blade-vortex interaction study are examined for influences of the three-dimensional rotor tip flows. Pressure data collected near the rotor tip are found qualitatively and quantitatively similar to corresponding data from more inboard locations. Differences between data collected near the tip and at more inboard locations are noted, and serve to highlight three-dimensional qualities of flows generated near the rotor tip. Data collected near the rotor tip during oblique interactions reveals the combined effects of the oblique intersection angle and of the tip-generated flows noted during parallel interactions.

2 Nomenclature

c	blade chord length
C_{mQC}	quarter chord moment coefficient
C_n	normal force coefficient
C_p	pressure coefficient
C_t	tangential force coefficient
r	radial position of pressure measurement pod
R	blade radius
R_e	Reynolds number
t	time
V_x	chordwise velocity at the measurement position at mid-interaction ($X_v/c=0.5$)
X_v	horizontal distance between the leading edge pressure transducer and the vortex centre, measured perpendicular to the vortex core
Y_v	vertical displacement of the vortex generator junction above the rotor disk
Z_v	lateral displacement of the vortex generator from the tunnel centreline
Γ	vortex circulation
Ω	angular velocity of the rotor blade
Ψ	blade azimuth angle

3 Introduction

Under certain conditions of powered descent or vigorous manoeuvring, rotorcraft blades pass through the wake and trailed tip vortices from previous blades (see Fig. 1). This interaction of the rotor blade with the tip vortex of a preceding blade is a significant source of noise and vibration in rotorcraft[1-3]. The need to reduce these undesirable effects requires that the rotorcraft designer has a clear appreciation of the contemporary fluid dynamic descriptions of phenomena underlying blade-vortex interaction. This need has been addressed through both experimental[4-27] and computational[28-31] studies attempting to isolate the BVI from the rotor environment.

While many of these BVI studies confine themselves to steady-state[19] or nominally two-dimensional[20-30] examinations of the blade-vortex interaction, only a few have considered the three-

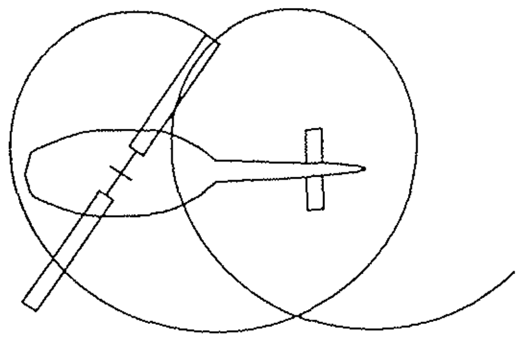

Fig. 1: Schematic of a rotorcraft experiencing blade-vortex interaction near the tip of the rotor blade.

dimensional tip flows of a finite wing and a free vortex.[4-11]. Both the Surendraiah[4]/Padakannaya[5] experiments and the experiment of Caradonna et al[6-8] isolated the BVI in wind tunnel tests involving an upwind vortex generating wing tip and a downwind rotor. The method employed in these studies allows examinations of the effects of the interaction upon tip flows. The Surendraiah/Padakannaya experiments exhibited great ingenuity in pioneering this approach, but suffered from a scarcity of pressure transducers and automatic data processing, thus weakening the resolution of C_p and C_n data, and unfortunately rendering C_m and C_t data virtually unobtainable. Caradonna et al presented experimental data only in C_p form, leaving many of the interesting facets of the integrated force coefficients unexplored. *In a corresponding computational* investigation[8] Caradonna et al generated C_n and C_m data for blade sections near the tip, but omitted direct comparisons with data from inboard span locations.

The Glasgow University BVI facility isolates the BVI in a manner similar to that used by Surendraiah, Padakannaya and Caradonna et al. The quality of pressure data collected, however, has allowed a preliminary investigation of the effects of tip flows upon the integrated aerodynamic coefficients. In addition, the large test matrix, incorporating measurements at several span locations during many different parallel and oblique interactions, has allowed comparison of near-tip and inboard BVI data, thus highlighting the effects of three-dimensional test conditions over those of the nominally two-dimensional state.

4 Methods

Experiments were conducted in the University of Glasgow "Handley Page" wind tunnel. An untwisted, non-lifting, single blade rotor interacted in a parallel or oblique mode with an oncoming vortex generated upstream of the rotor disk by a stationary wing. This set-up is depicted in Fig. 2.

The rotor blade had a NACA 0015 aerofoil section, *with a 0.149 m chord and a 0.9426 m radius.* An instrumented pod containing 26 miniature pressure transducers (3 KULITE XCS-093-5-SG transducers and 23 ENTRAN-EPIL-080B-5S transducers) was fitted into the blade at one of 5 spanwise positions. The most outboard of these positions (94.5% radius) was used during examinations of flows near the rotor tip. During tests the voltages from the 26 pressure transducers were amplified, low-pass filtered, and then simultaneously digitised (using a Thorn EMI BE256-420 data logger)

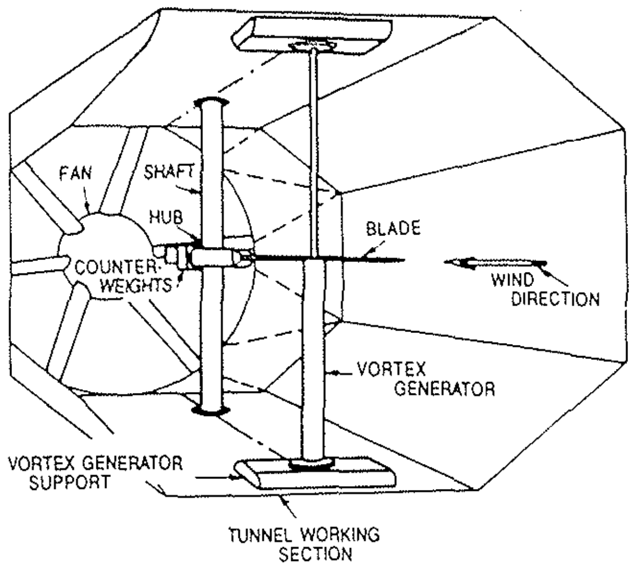

Fig. 2: The new Glasgow University BVI facility in the Handley Page wind tunnel.

before being stored in an IBM PS/2 80/041 computer for further reduction and presentation. Data collection was locked to azimuth position, and each test run comprised the collection of data during many (typically 7) interactions. Data were subsequently ensemble averaged about the C_n cross over point (see ref. 16), the point near $X_v/c = 0.0$, where the normal force drops through zero, between the peak and the nadir in C_n.

The vortex generator was made of two adjoining NACA 0015 aerofoil sections spanning the height of the test section 2.1 rotor radii upstream of the rotor hub. The vortex strength was controlled by setting the two sections at equal but opposite incidence. The magnitudes of the vortex strength were identical to those used by Kokkalis and Galbraith[9,10], who measured vortex circulation by means of a triple hot-wire probe. The horizontal position of the vortex generator (Z_v) determined the angle of intersection between the interaction vortex and the blade, resulting in either a parallel or oblique BVI. The vertical position of the aerofoil junction on the vortex generator (Y_v) was altered to vary the height of the interaction vortex above the rotor disk. A schematic of the test rig, indicating the positive directions of X_v, Y_v, and Z_v, is presented in Fig. 3. The full test matrix is presented in Table 1.

During tests the rotor and vortex generator were situated together in the 1.61 x 2.13 m octagonal test section. The tunnel was run at 47.0 m/s, while the rotor was rotated with a tip speed of 59.3 m/s. The

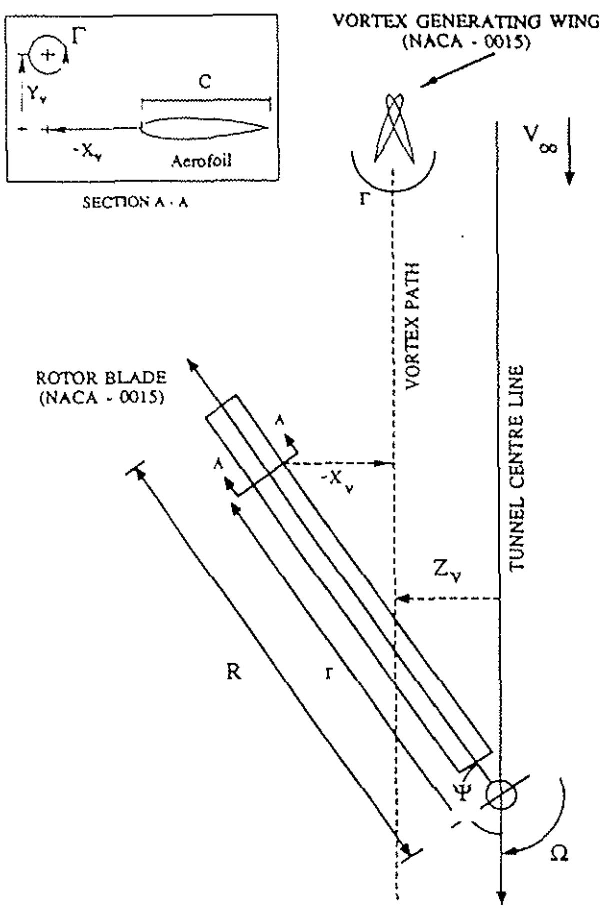

Fig. 3: A schematic of the blade-vortex interaction rig, indicating the positive directions for X_v, Y_v, and Z_v.

	r/R = 0.944	r/R = 0.865	r/R = 0.785	r/R = 0.706	r/R = 0.626
Zv/c = 2	$\bar{c}$ =0.630	$\bar{c}$ =0.660	$\bar{c}$ =0.691	$\bar{c}$ =0.718	$\bar{c}$ =0.743
Zv/c = 1	$\bar{c}$ =0.707	$\bar{c}$ =0.754	$\bar{c}$ =0.806	$\bar{c}$ =0.863	$\bar{c}$ =0.923
Zv/c = 0 (parallel)	$\bar{c}$ =0.804 0.612 0.408 0.264 0.132	$\bar{c}$ =0.878 0.668 0.446 0.288 0.144	$\bar{c}$ =0.967 0.736 0.491 0.318 0.159	$\bar{c}$ =1.076 0.819 0.546 0.353 0.177	$\bar{c}$ =1.213 0.923 0.615 0.398 0.199
Zv/c = -1	$\bar{c}$ =0.936	$\bar{c}$ =1.055	$\bar{c}$ =1.214	$\bar{c}$ =1.438	$\bar{c}$ =1.784
Zv/c = -2	$\bar{c}$ =1.110	$\bar{c}$ =1.319	$\bar{c}$ =1.620	$\bar{c}$ =2.147	$\bar{c}$ =3.293

Table 1. A test matrix of the parallel blade-vortex interactions examined. All cases were tested at eleven values of vortex aerofoil separation height: Y_v/c = 1.0, 0.8, 0.6, 0.4, 0.2, 0.0, -0.2, -0.4, -0.6, -0.8, -1.0.

comparable aerodynamic scaling of the vortex generator and the rotor assured a realistically scaled BVI.

Pressure data were integrated around the aerofoil section to provide force and moment data. Pressure, force and moment data were nondimensionalised into aerodynamic coefficients using the local chordwise velocity at the measurement location when $X_v/c = 0.5$. The nondimensional time variable, X_v/c was computed from the geometry of the blade and does not account for BVI induced perturbations to the vortex position. More detail on the experimental set-up and procedure may be found in Horner et al[16].

5 Results

During tests, pressure data were collected at 26 locations around the chord of a test aerofoil during interaction with a free vortex. The pressure and integrated force data collected near the rotor blade tip showed many of the same features observed in data collected at inboard locations. Pressure data were dominated by the build up of the leading edge suction peak during the approach of the interaction vortex, while normal force data were characterised by the associated build up and then sudden reversal of C_n. Pressure, force and moment histories from near the tip exhibited variations in magnitude and alterations in form from that observed at inboard sections.

An example of typical averaged data measured near the rotor tip (at 94.5% span) during a parallel interaction is presented in Fig. 4. The interaction vortex was generated 0.2 chord lengths below the rotor disk, and had a strength of 6.7 m^2/s. Fig. 4 presents the data for this test in five plots: two plots depicting the pressure profile histories of the upper and lower aerofoil surfaces, and three curve plots presenting the time histories of the integrated aerodynamic coefficients: C_n, $C_{m_{QC}}$, and C_t. The surface plots are made up of a stacked sequence of chordwise pressure distributions. The first pressure distribution, representing data taken at Xv/c = -1.816, is in the foreground of each surface plot. On the upper surface plot this initial pressure distribution is shaped in a manner suggestive of the suction side of an aerofoil, reflecting the increasing incidence produced by the approaching vortex. Similarly, the initial pressure distribution in the lower surface plot reflects the higher pressures expected of the pressure side of the aerofoil. Subsequent pressure distributions show increases in the leading edge suction peak (on the upper surface) and corresponding increases in lower surface pressure associated with the approach of the vortex. As the

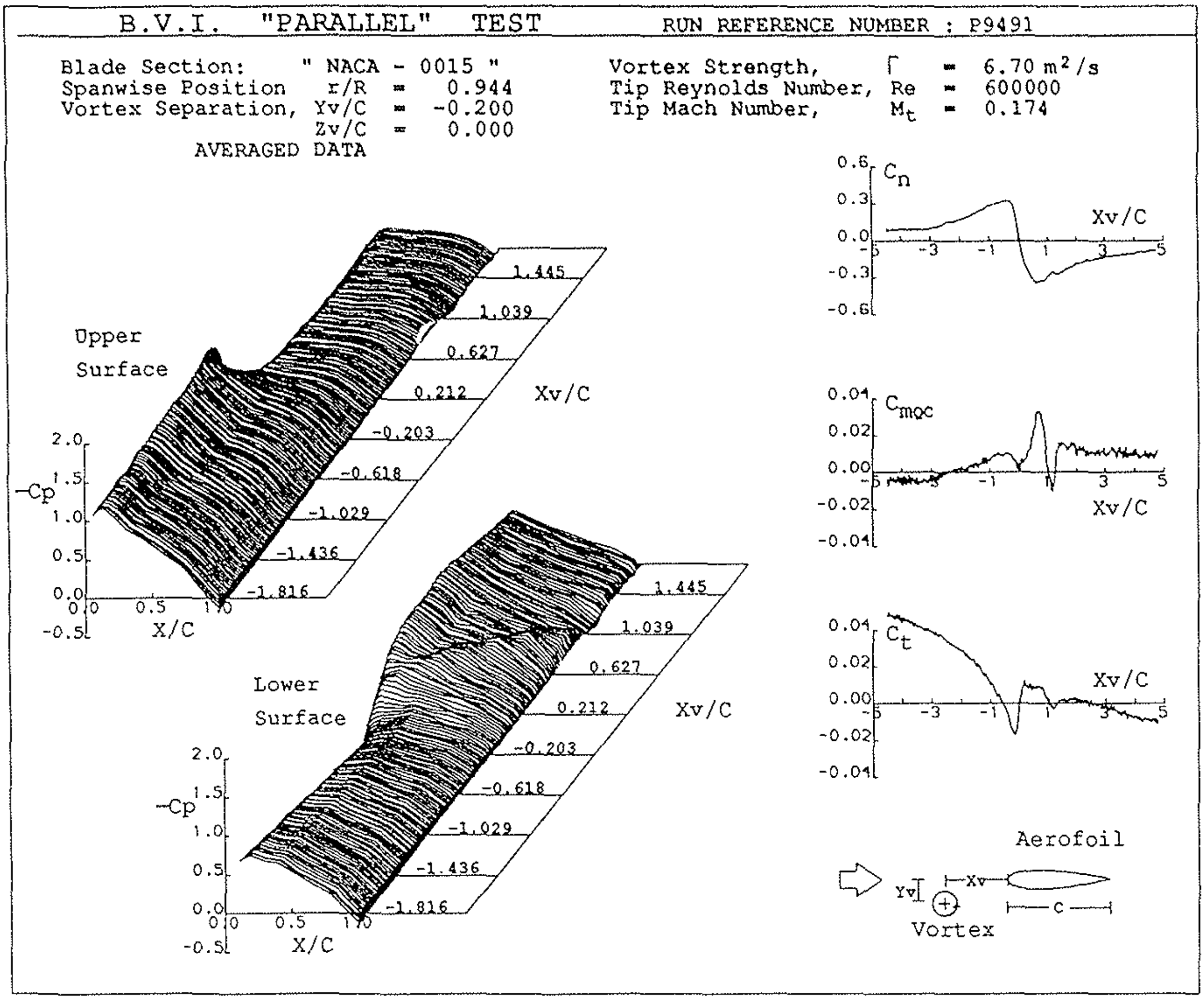

Fig. 4: Typical data from a parallel blade-vortex interaction near the blade tip. $\Gamma = 6.7 m^2/s$, $r/R = 0.945$, $Y_v/c = -0.2$.

vortex passes under the leading edge near $X_v/c = 0.0$, the leading edge suction peak (upper surface) collapses, and a region of increased suction begins to build near the leading edge of the lower surface. As the interaction continues a smaller suction ridge slants away towards the trailing edge of the aerofoil lower surface. This ridge marks the "convective disturbance" that has been associated with the proximity of the vortex as it traverses the lower surface[7,8,18]. After this disturbance passes the trailing edge near $X_v/c = 1.0$, the pressure distributions take on the character of those associated with an aerofoil at negative incidence.

The C_n data (Fig. 4) follow the same general sequence described by Surendraiah[4]. During the first half of the C_n history, the normal force is seen to rise towards a peak value of 0.33, as the approach of the vortex produces an increase in incidence and a growth in the leading edge suction peak on the upper surface. The collapse of this suction peak, and the reversal of incidence as the vortex passes the leading edge, is reflected in the precipitous drop in C_n near $X_v/c = 0.0$. The ensuing negative lift is briefly reduced when the low pressure "convective disturbance" ridge passes from the lower surface; a short pressure pulse on the lower surface near the trailing edge further reduces this negative lift. The resulting perturbation in the C_n curve has been reported in previous experimental and computational studies of blade-vortex interaction[18,30]. Following this C_n perturbation the normal force converges towards zero as the vortex convects further downstream.

The quarter chord moment coefficient history is presented below the C_n data. The initial rise in C_m, culminating in a peak near Xv/c = -0.5, presumably reflects a disproportionate growth of the leading edge suction peak resulting from the disparity in vortex induced incidence between the leading and trailing edges. The effect of the leading edge suction peak gives way to the effect of the low pressure vortex "disturbance", which pulls down first on the leading edge, briefly neutralising the moment, and then pulls down on further aft positions, quickly raising C_{mQC} to the maximum value attained. The passage of the low pressure "disturbance" off of the lower surface, and the subsequent pressure pulse on the lower surface, precipitously drop the moment from its maximum value to its minimum. This nadir in the C_m history is similar to that previously noted at inboard locations[18]. This minimum value is as transient as the positive pressure pulse, for it disappears quickly, leaving a positive moment which subsequently converges towards zero.

The tangential force history is dominated by the large forward force generated by the approaching vortex. This force peaks as the vortex approaches the leading edge of the aerofoil, and then abruptly reverses once the vortex passes the leading edge. A second minimum in tangential force near X_v/c = 1.0 corresponds with the trailing edge pressure pulse seen in the pressure plots, suggesting that this decrease in tangential force is due to the departure of the "convective disturbance" from the lower surface of the aerofoil.

In order to highlight the effect of tip flows inherent in the data of Fig. 4, this data set is compared to comparable inboard data in Fig. 5. These data reflect a parallel interaction with a vortex of circulation Γ = 6.7 m^2/s passing 0.2 chords below the blade. The data depicted by the square symbols is that at 94.5% span, already presented in Fig. 4, whilst the diamond symbols depict data collected at 86.5% span.

The normal force histories for these interactions are presented in the top plot. Throughout the approach of the vortex the normal forces measured near the tip remain lower than those measured inboard. The tip C_n data reach a peak value of 0.33 (compared with 0.39 inboard) and then both curves drop through zero as the vortex passes the leading edge. Subsequently both curves attain comparable minimum values (-0.34 near the tip, -0.33 inboard) before tending towards zero as the vortex convects into the wake.

The middle plot in Fig. 5 presents the C_m histories. Unlike C_n, C_m histories show significant

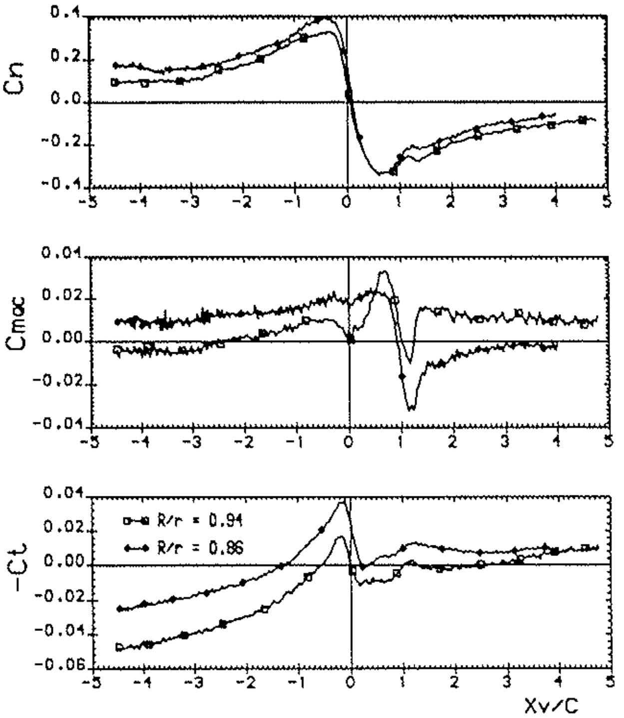

Fig. 5: Comparison of aerodynamic coefficients collected at inboard and near-tip locations during parallel interactions.
Γ = 6.7m^2/s, Y_v/c = -0.2

qualitative differences in form when measured near the tip. During the approach of the interaction vortex, the tip C_m values are negative, while those measured inboard are positive. Both C_m curves rise during the approach of the vortex, reflecting the effect of the growing leading edge suction peak, and both curves show a dip near X_v/c = 0.0, when the low pressure vortex passes just below the leading edge. Throughout these portions of the interaction, however, the tip C_m remains lower than that measured inboard. After the vortex passes the quarter chord, the associated suction effects an increase in quarter chord moment, and both curves climb towards their respective maximum. While this increase is modest in inboard locations, it is substantial near the tip, causing the tip moment data to surpass the inboard data. For the remainder of the interaction the tip data remains greater than that from inboard. Near X_v/c = 1.0 both curves show the brief but strong negative spikes previously associated with the trailing edge passage of the interaction vortex[18]. Subsequently both curves tend towards zero, but the tip data approaches zero from the positive side, while the inboard data converges from the negative side. It is apparent that throughout the interaction the two curves follow a similar series of maxima and minima, however the tip data cross from being consistently less than the inboard data to being

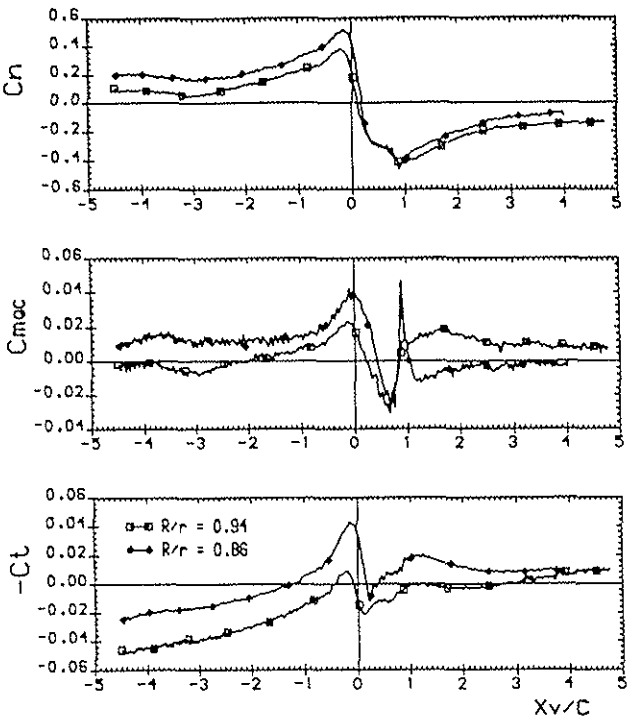

Fig. 6: Comparison of aerodynamic coefficients collected at inboard and near-tip locations during parallel interactions.
Γ = 6.7m²/s, Y_v/c = 0.2

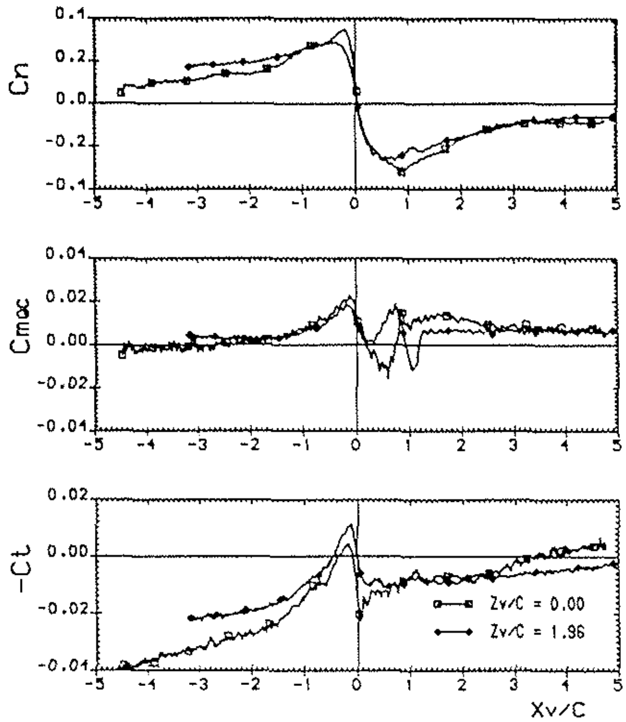

Fig. 7: Comparison of aerodynamic coefficients collected near the blade tip during parallel and 2nd quadrant oblique interactions. Both cases measured at r/R = 0.945, with Y_v/c = 0.2. Γ = 6.7m²/s during oblique test, Γ = 5.1m²/s during parallel test.

consistently greater in the single large increase in C_m observed between Xv/c = 0.0 and 0.7.

The lower plot in Fig. 5 presents the tangential force histories. In both curves the dominant feature is the peak in forward force as the vortex approaches the leading edge of the blade. During the build-up in forward force the inboard -Ct values are consistently greater than those measured near the tip. The two curves draw nearer after the forward force peaks drop off, near Xv/c = 0.2. subsequently the inboard -Ct values increase faster than those observed near the tip, so that the curves are farther apart near Xv/c = 0.8. Both curves show an increase in forward force as the vortex convects past the trailing edge, apparently due to the corresponding reduction in suction on the aft portion of the aerofoil. Subsequently the curves converge as the vortex convects downstream.

Because the form of force and moment histories has been shown to differ for interactions with vortices passing above or below the test aerofoil, comparisons between tip and inboard data are also presented for interactions with positive Y_v/c. In Figure 6 inboard and near-tip data are compared for a parallel interaction similar to that of Fig. 5, except that the interaction vortex passes above the test aerofoil. The data are for a vortex strength of 6.7 m²/s and a separation height (Y_v/c) of 0.2. The comparisons in these three plots highlight trends similar to those observed in Fig. 5. Again, the near-tip C_n values rise to a lower peak than measured inboard, and subsequently attain a comparable minima.

The comparison of near-tip and inboard C_m curves in the middle plot of Fig. 6 highlights tip effects similar to those noted in Fig. 5. Again the near-tip and inboard moment curves follow similar sequences of peaks and valleys, with the tip C_m values initially less than those from inboard, but crossing and surpassing the inboard curve while the vortex is above the blade, and remaining positive during the convection of the vortex into the wake. In this case, unlike the case of Fig. 5, the C_m spike associated with the trailing edge passage of the vortex is significantly suppressed in the case of the near-tip data.

The comparison of tangential force data in the lower plot of Fig. 6 also highlights the same sort of tip effects noted in Fig. 5 . Again the pressure drag is greater near the tip than inboard, and again this difference is least just after the vortex passes the leading edge. The similarity of the tip effects noted in Fig. 6 to those noted in Fig. 5 serves to underscore the consistent effects of tip flows upon a variety of different BVI geometries.

In order to asses the effects of tip flows upon the previously noted[17] effects of variation in intersection angle, Fig. 7 compares parallel and oblique interactions using data collected near the rotor tip. The diamond symbols denote data from an oblique interaction ($Zv/c = 1.96$) with the strongest vortex ($\Gamma = 6.7\ m^2/s$), resulting in a nondimensional vortex strength of 0.630. The square symbols denote data from a parallel interaction with a weaker vortex ($\Gamma = 6.7\ m^2/s$), resulting in a nondimensional vortex strength of 0.612. Both interactions were with a vortex originating 0.2 chord lengths above the rotor disk. In the upper plot, a comparison of normal force histories reveals that in the early stages the oblique interaction has larger C_n values. Subsequently the oblique case C_n values climb more slowly than in the parallel case, have a lower and more rounded peak, and drop towards a negative value slightly less steeply than in the parallel case. After the interaction vortex has passed the trailing edge the two curves show rapid convergence, and are almost indistinguishable as the vortex convects into the wake. The C_m and C_t curves show a similar response to the final approach of the vortex, with the coefficients showing a more rounded peak under oblique interaction conditions than under parallel conditions. In the case of C_m this peak is higher in the oblique test, but in the C_t plot, as in the C_n plot, the parallel test produces the highest peak. The alterations in data in Fig. 7 resulting from the oblique geometry are qualitatively similar to the effects of alterations in intersection angle noted at inboard locations in Ref. 17.

6. Discussion

The pressure measurements taken near the rotor tip during blade-vortex interactions were found to be similar to those collected at more inboard locations. Pressure data from all span locations were dominated by the buildup and subsequent collapse of the leading edge suction peak, and the associated build-up and reversal of the integrated normal force coefficients. These prominent features of the pressure and integrated force data show a large degree of qualitative and quantitative similarity with the results of previous studies, both experimental and computational (see ref. 16 for data comparisons). Despite these gross similarities, pressure, force, and moment histories collected near the rotor tip showed subtle but significant alterations in form and variations in magnitude when compared with data collected inboard. These differences between inboard and tip data highlight the added complexity of the three-dimensional flows present near the rotor tip.

The comparisons between inboard and near-tip data presented in Figs. 5 and 6 serve to highlight three prominent effects of tip flows during blade-vortex interactions:

1) Differences in the magnitudes of C_n peaks attained at inboard and near-tip locations suggest that flows near the rotor tip effect the same sort of reductions in incidence expected near finite wing tips.

2) C_m and C_t histories recorded near the rotor tip reveal qualitatively similar alterations to pressure distributions across a variety of interaction geometries. These alterations are consistent with the expected local effects of a rotor tip vortex.

3) The C_m perturbation associated with vortex-trailing edge passage (near $Xv/c = 1$) is reduced by tip flows, but only in cases when the vortex passes above the blade. This suggests that this effect may result from vortical interactions between the tip and interaction vortices, in which the sense of the vorticity is important in determining the effect on the pressure data..

In order to asses the nature of the incidence changes suggested by Point 1 above, a broader survey of C_n behaviour is necessary. Figure 8 presents a summary of maximum C_n attained during BVI against the nondimensional vortex strength of the interaction vortex used in each test. The data presented is for parallel

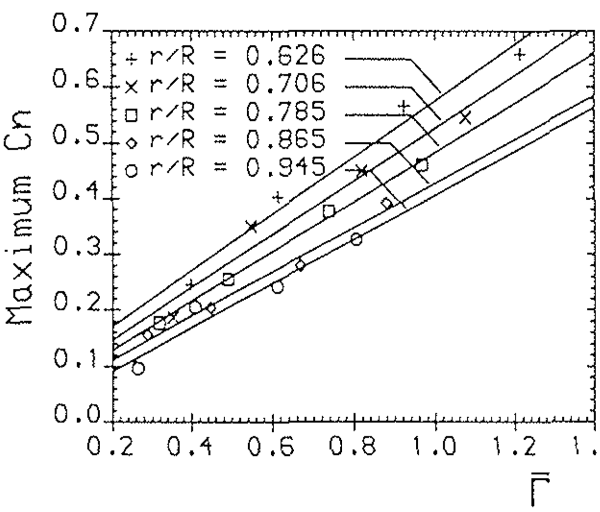

Fig. 8: A plot of the maximum Cn obtained vs. nondimensional vortex strength. Data are grouped by span location. $Zv/c = 0$ and $Yv/c = -0.2$ in all cases.

interactions with the vortex originating 0.2 chord lengths below the rotor disk, and includes only the strongest four vortex strengths tested. (The C_n max. values from Fig. 5 are indicated by the highest diamond and circle symbols, for data from the 86% and 94% span locations, respectively.) A line fit through the data points from each span location is included to aid in comparisons of the data from different span positions. It is evident from Fig. 8 that at each span location increases in the nondimensional vortex strength result in nearly linear increases in peak C_n. It is also evident from this plot that the effects of increased vortex strength are reduced at more outboard locations. Both of these observations are consistent with the observations of Horner et al[17], who noted similar trends across a variety of parallel and oblique interactions for all inboard locations. As noted in this previous study, such variations in peak C_n are compatible with the reductions in incidence expected of the tip vortex in outboard locations[32].

The variations in C_m and C_t noted in Point 2 above are only evident in the most outboard measurement position, and indicate further differences in tip flows independent of the phenomena of Point 1. It is evident in the C_m histories of Figs. 5 and 6 that the tip flows reduced C_m to negative values during the approach of the interaction vortex, and raised C_m to positive values during the downstream convection of the interaction vortex following the BVI. This alteration in C_m would be consistent with a suction influence upon the aft portion of the upper surface while incidence is positive (during the approach of the interaction vortex) and upon the aft portion of the lower surface while the incidence is negative (following the passage of the interaction vortex).

Such increases in aft suction would be consistent with the type of pressure perturbations effected by a vortex trailing from a finite wing tip[32] were it to cross the aft portion of the outboard measurement position. Previous studies have shown that for both steady state[32] and unsteady[33-36] conditions, the tip vortex emanates from the leading edge of the wingtip, and slants inboard over the suction surface before trailing into the wake.

In order to asses the spatial relationships of flow structures near the tip a diagram of the interaction geometry is given in Fig. 9. This figure presents a scale view of the test rotor together with local velocity vectors for a variety of test conditions while the rotor is at an azimuth position of 180°. It is apparent from Fig. 9 that if the tip vortex emanates from the leading edge, and

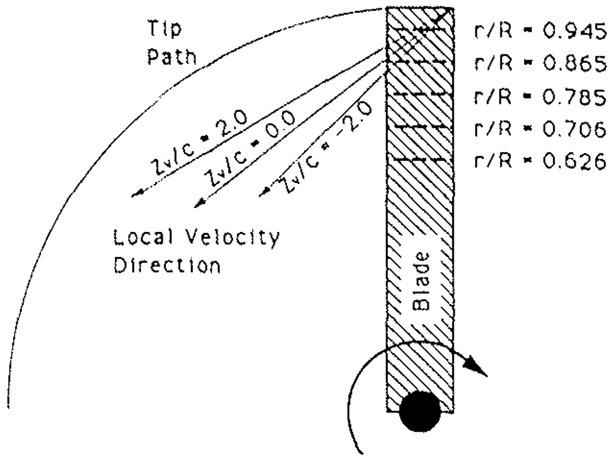

Fig. 9: Schematic of flow velocities near the blade tip.

crosses the suction surface inboard of the tip path, near the local velocity vector, it will pass close to the aft portion of the 94.5% span location.

A caricature of this positioning of the tip vortex is presented in Fig. 10, for a parallel BVI with the interaction vortex passing below the rotor disk. The lower pressures expected in the proximity of the tip vortex would be expected to increase the suction in aft regions of the blade near the tip vortex, as indicated in

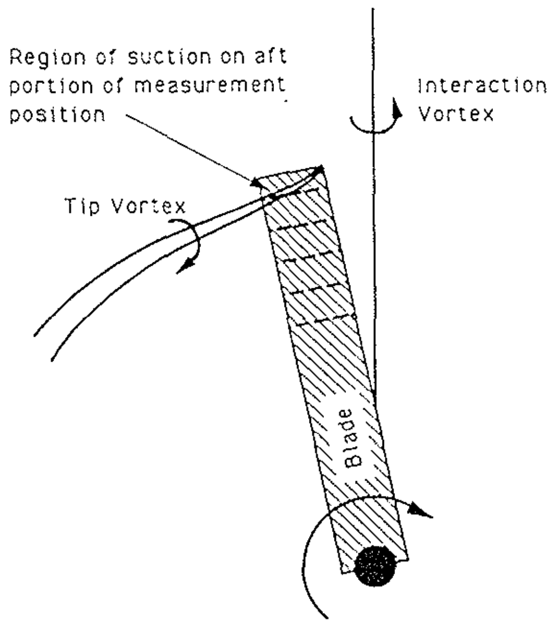

Fig. 10: Caricature of vortical flows near the blade tip during blade-vortex interactions. $Y_v/c < 0$, $X_v/c < 0$.

this figure. The result of this increase in suction over the aft portion of the aerofoil upper surface would be a reduction in C_m already noted.

Once the vortex passes the aerofoil (X_v/c greater than zero), the incidence on the blade reverses, and the tip vortex would be expected to cross the lower surface (now the suction surface). The sense of the tip vortex would also be opposite to that expected at positive incidence. A schematic of this geometry is depicted in Fig. 11. The region of low pressure effecting the outboard measurement position is indicated on the rear portion of the measurement position. The result of this increase in aft suction on the lower surface would be the more positive C_m values observed in later portions of the data.

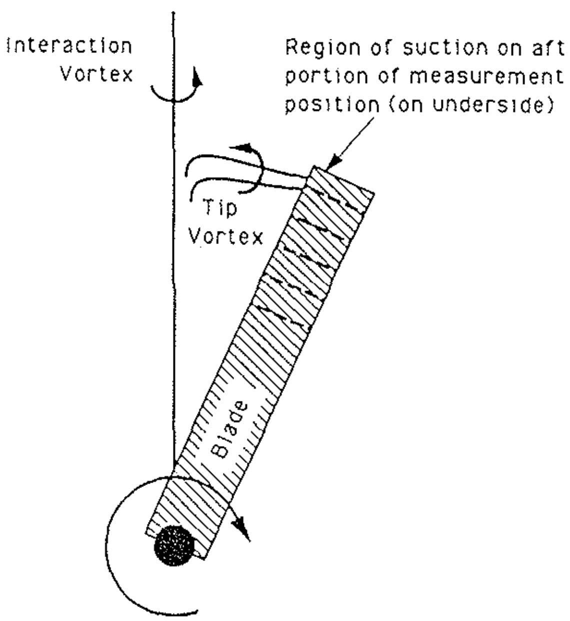

Fig. 11: Caricature of vortical flows near the blade tip during blade-vortex interactions. $Y_v/c < 0$, $X_v/c > 0$.

The increased suction on the aft portions of the aerofoil resulting from the proximity of a trailing tip vortex would also enhance C_t in tip regions during periods of both positive and negative incidence. The extra pressure drag noted in Figs. 5 and 6 would be consistent with the expected suction indicated in Figs. 10 and 11. The brief convergence of the tip and inboard C_t curves near $X_v/c = 0.2$ would then correspond to the time of transition from positive to negative incidence, during which the tip vortices might be expected to be at their weakest.

As indicated in Point 3 above, tip flows effect a reduction in the vortex-trailing edge passage perturbation in the Cm history in all interactions with vortices passing above the blade (see Figs. 6 and 7). The observation that this alteration only appears in the case of the vortex passing above the blade suggests that the induced flows from the tip vortex are countering the flows with which interaction vortex normally instigates this perturbation. It is possible that the mechanism by which the tip vortex counters this perturbation involves the lifting of the interaction vortex farther above the blade when the interaction vortex passes above the aerofoil. Further insight into the fluid mechanisms behind this effect will require flow visualisation of trailing edge flows near the rotor tip.

In addition to comparisons of data collected with or without tip effects, the present data set allows an assessment of the effects of tip flows upon the previously described[17] effects of variations in intersection angle. The comparisons of Fig. 7, between data from parallel and oblique interactions, highlight the same effects of altering the blade-vortex intersection angle that were noted at all other span locations by Horner et al[17]. In this previous study it was suggested that the alterations to the integrated force and moment histories, particularly the normal force history, are due to the generation of vortical flow structures trailing from the spanwise position of intersection between the blade and the interaction vortex. Because the alteration of BVI intersection angle results in the same changes to data whether measured inboard or near the tip, it appears that the effects of tip flows and the effects of the three-dimensional flows arising from oblique interactions can be considered independently, and appear to act in combination in the case of oblique interactions examined near the rotor tip.

7 Conclusion

The pressure histories measured about the test aerofoil during the blade-vortex interactions examined in this study revealed many qualitative and quantitative similarities between data collected at inboard and near-tip locations. The rise and collapse of the leading edge suction peak appeared similar at all locations, as did the convective disturbances associated with the close passage of the interaction vortex. The force and moment data integrated from the pressure histories also maintained a similar sequence of features under parallel and oblique conditions.

The magnitudes of the peaks, valleys and perturbations of all data were strongly dependent upon the nondimensional vortex strength used during test runs. This appeared particularly true for normal force data, where a nearly linear relation between

C_n maximum and nondimensional vortex strength was noted. Peak C_n values were also found to vary with spanwise position, with more outboard locations yielding lower values of C_n maximum. This spanwise variation in C_n data was found consistent with the expected incidence changes effected by the tip vortex.

Other effects of the tip flows were only noted for data measured at the most outboard measurement location and served to further highlight the three-dimensional nature of the flows generated near the tip during blade vortex interactions. The alterations to C_m and C_t data effected by tip flows were found consistent with the expected effects of the proximity of a trailed tip vortex. Alterations in the effects of vortex-trailing edge passage were also noted in interactions with vortices passing beneath the outboard measurement location.

The effects of varying the blade-vortex intersection angle were found similar at all measurement positions examined. The data collected at the near-tip measurement position during oblique interactions appeared to exhibit the superposition of tip effects noted in this study together with the oblique effects noted in a previous examination of oblique interactions[17]. This implies that different aspects of the three dimensional BVI flow structures are responsible for near-tip and oblique interaction alterations in data.

8 Acknowledgements

The authors would like to acknowledge the support of the British Ministry of Defence, and the Defence Research Agency (formerly RAE). The help of Westland Helicopters, in particular T. Beddoes, during the design and execution of the experiment was appreciated. The authors would also like to thank Dr. M. Luttges and Dr. M. Robinson of the Dept. of Aerospace Engineering Sciences of the University of Colorado, Boulder, for their support.

References

1. Scheiman, J. and Ludi, L.H., "Qualitative Evaluation of Effect of Helicopter Rotor-Blade Tip Vortex on Blade Airloads"NASA TN D-1637, May, 1963.

2. Brotherhood, P., and Riley, M.J., "Flight Experiments on Aerodynamic Features Affecting Helicopter Blade Design", Vertica, Vol. 2 , pp. 27-42, 1978.

3. Schmitz, F.H., Boxwell, D.A., Lewy, S., and Dahan, C., "Model- to Full-Scale Comparisons of Helicopter Blade-Vortex Interaction Noise", 38th Annual National Forum of the American Helicopter Society, Anaheim, Calif., May, 1978.

4. Surendraiah, M. "An Experimental Study of Rotor Blade-Vortex Interaction", M.S. Thesis, The Pennsylvania State University, December, 1969.

5. Padakannaya, R. "Experimental Study of Rotor Unsteady Airloads due to Blade Vortex Interaction", NASA CR - 1909, November, 1971.

6. Caradonna, F.X., Laub, G.H. and Tung, C. "An Experimental Study of Rotor-Vortex Interaction", NASA TM-86005, November, 1984.

7. Caradonna, F.X., Lautenschlager, J.L. and Silva, M.J., "An Experimental Study of Rotor-Vortex Interactions", AIAA Paper 88-0045, AIAA 26th Aerospace Sciences Meeting, Reno, Nevada, January, 1988.

8. Caradonna, F.X., Strawn, R.C., and Bridgeman, J.O.,"An Experimental and Computational Study of Rotor-Vortex Interactions",14th European Rotorcraft and Powered Lift Aircraft Forum, Milano, Italy, September, 1988.

9. Kokkalis, A. and Galbraith, R.A.McD. "Description of, and Preliminary Results from, a New Blade-Vortex Interaction Test Facility", 12th European Rotorcraft and Powered Lift Aircraft Forum, Garmisch - Partenkirchen, Federal Republic of Germany, September, 1986.

10. Kokkalis, A. and Galbraith, R.A.McD. "Results from the Glasgow University Blade-Vortex Interaction Facility", 13th European Rotorcraft and Powered Lift Aircraft Forum, Arles, France, September, 1987.

11. Saliveros, E. and Galbraith, R. A. McD. "Collected Data from Blade Vortex Interaction Tests Using a Single Blade, Non-Lifting Rotor ; Vol. I : 94% Span" G.U. Aero Report 9007, Glasgow University, March, 1990.

12. Saliveros, E. and Galbraith, R. A. McD. "Collected Data from Blade Vortex Interaction Tests Using a Single Blade, Non-Lifting Rotor; Vol. II : 86% Span" G.U.Aero Report 9008, Glasgow University, March, 1990.

13. Saliveros, E. and Galbraith, R. A. McD.
"Collected Data from Blade Vortex Interaction Tests Using a Single Blade, Non-Lifting Rotor; Vol. III: 78% Span" G.U. Aero Report 9009, Glasgow University, March, 1990.

14. Saliveros, E. and Galbraith, R. A. McD.
"Collected Data from Blade Vortex Interaction Tests Using a Single Blade, Non-Lifting Rotor; Vol. IV: 70% Span" G.U. Aero Report 9010, Glasgow University, March, 1990.

15. Saliveros, E. and Galbraith, R. A. McD.
"Collected Data from Blade Vortex Interaction Tests Using a Single Blade, Non-Lifting Rotor; Vol. V: 62% Span" G.U. Aero Report 9011, Glasgow University, March, 1990.

16. Horner, M.H., Saliveros, E., Kokkalis, A., and Galbraith, R.A.McD., "Results from a Set of Low Speed Blade-Vortex Interaction Experiments", Glasgow University Aero Report 9109, July, 1991.
To be published in Journal of Experiments in Fluids

17. Horner, M.H., Saliveros, E., and Galbraith, R.A.McD., "An Experimental Investigation of the Oblique Blade-Vortex Interaction", 17th European Rotorcraft and Powered Lift Aircraft Forum, Berlin, Germany, September, 1991.

18. Horner, M.H., Saliveros, E., and Galbraith, R.A.McD., "An Examination of Vortex Convection Effects During Blade-Vortex Interaction", AHS/RAeS Technical Specialists Meeting on Rotorcraft Acoustics and Rotor Fluid Dynamics, Philadelphia, U.S.A., October, 1991.

19. Seath, D.D.
"Vortex-Airfoil Interaction Tests", 2nd Atmospheric Flight Mechanics Conference, Palo Alto and Moffett Field, California, September, 1972.

20. Seath, D.D., Kim, J.M. and Wilson, D.R.
"An investigation of the Parallel Blade-Vortex Interaction in Low-Speed Wind Tunnel", AIAA Paper 87-1345, AIAA 19th Fluid Dynamics, Plasma Dynamics and Lasers Conference, Honolulu,Hawaii, June, 1987.

21. Ham, N.D.
"Some Preliminary Results from an Investigation of Blade-Vortex Interactions", Journal of the American Helicopter Society, Vol. 19, pp. 45-48, April, 1974.

22. Ham, N.D.
"Some Conclusions from an Investigation on Blade-Vortex Interaction", Journal of the American Helicopter Society, Vol. 20, pp 26-31, October, 1975.

23. Booth, E.R. Jr. and Yu, J.C.
"Two-Dimensional Blade-Vortex Flow Visualisation Investigation", AIAA Journal Vol. 24, No. 9, September, 1986.

24. Booth, E.R. Jr.
"Surface pressure Measurement During Low Speed Two-Dimensional Blade Vortex Interaction", AIAA Paper 86-1856, AIAA 10th Aeroacoustics Conference, Seattle, Washington, July, 1986.

25. Meier, G.E.A. and Timm, R.
"Unsteady Vortex Airfoil Interaction"
AGARD CP - 386, May, 1985.

26. Straus, J., Renzoni, O. and Mayle, R.E.
"Airfoil Pressure Measurements During a Blade-Vortex Interaction and a Comparison with Theory",AIAA Paper 88-0669, AIAA 26th Aerospace Sciences Meeting, Reno, Nevada, January, 1988.

27. Huyer, S. A., and Luttges, M. W.
"Unsteady Flow Interactions Between the Wake of an Oscillating Airfoil and a Stationary Trailing Airfoil", AIAA Paper 88-2581, AIAA 6th Applied Aerodynamics Conference, Williamsburg, Virginia, June 1988.

28. Sears, W.R.
"Aerodynamics, Noise and the Sonic Boom", AIAA Journal, Vol. 7, No. 4, April, 1969.

29. Panaras, A.
"Numerical Modelling of the Vortex-Airfoil Interaction", AIAA Journal, Vol. 25, No. 1, January, 1987.

30. Lee, D.J. and Smith, C.A.
"Distortion of Vortex Core during Blade/Vortex Interaction", AIAA Paper 87-1243, AIAA 19th. Fluid Dynamics, Plasma Dynamics & Lasers Conference Honolulu, Hawaii, June, 1987.

31. Jones, H.E., and Caradonna, F.X.,
"Full Potential Modelling of Blade-Vortex Interactions", Vertica Vol. 12 No. 1/2, pp. 129-145, 1988.

32. Chigier, N. A., and Corsiglia, V. R.
"Tip Vortices - Velocity Distributions"
NASA TM X-62,087, September 1971

33. Freymuth, P.
"Visualizing the Connectivity of Vortex Systems for Pitching Wings", Journal of Fluids Engineering, Vol. 111, June 1989.

34. Freymuth, P., Finaish, F., and Bank, W.
"Further Visualization of Combined Wing Tip and Starting Vortex Systems", AIAA Journal, Vol.25, No. 9, September 1987.

35. Horner, M. B., Addington, G. A., Young J. W., and Luttges, M. W.
"Controlled Three-Dimensionality in Unsteady Separated Flows About a Sinusoidally Oscillating Flat Plate", AIAA Paper 90-0689, 28th Aerospace Sciences Meeting, Reno, Nevada, January, 1990.

36. Robinson, M. C.
"Pitch Rate and Reynolds Number Effects on a Pitching Rectangular Wing", AIAA Paper 88-2577-CP, AIAA 6th Applied Aerodynamics Conference, Williamsburg, Virginia, June, 1988.